Mitochondria–cytoskeleton interactions in mammalian sperm revealed by cryoelectron tomography

Huafeng Wang[a] and Jean-Ju Chung[a,b,1]

The beginning of understanding sperm biology coincided with the design and invention of the light microscope in 1677 by Antonie van Leeuwenhoek. He was the first person to observe sperm cells, and described them as "small animals," because they move! Indeed, motility is one of the essential features of sperm cells for fertility. Introduction of electron microscopy (EM) in the midtwentieth century (1, 2) has also led to a dramatic leap in sperm biology, as sperm cells, the smallest cell types in the body, have submicron flagellar dimensions. EM and freeze-fracture studies enabled visualization of sperm subcellular structures (3). Our current understanding of cellular organization and processes underlying sperm capacitation and fertilization benefited greatly from advances in microscopy technologies and imaging methods. More recently, further techniques have been applied to sperm biology and fertilization research, including studies using superresolution light microscopy, tissue clearing and expansion microscopy, and cryo-EM (4–7). In PNAS, using cutting-edge cellular cryo-EM (Fig. 1*A*), Leung et al. (8) report structural diversity and conservation of mammalian sperm mitochondria in greater detail. Sperm mitochondria are tethered to each other through intermitochondrial linkers and to the underlying cytoskeleton through conserved protein arrays on the mitochondrial membrane (Fig. 1*B*).

In many specialized cell types, mitochondria are positioned to specific subcellular locations through interactions with the cytoskeleton (9). Typical mammalian sperm, which lose most of the cytoplasm and other organelles during the final stage of spermatogenesis, still retain ~50 to 75 mitochondria. In the flagellar region called the midpiece, these mitochondria form sheaths by wrapping helically around the cytoskeleton underneath, suggesting unique mitochondrial dynamics during flagellar formation. This arrangement

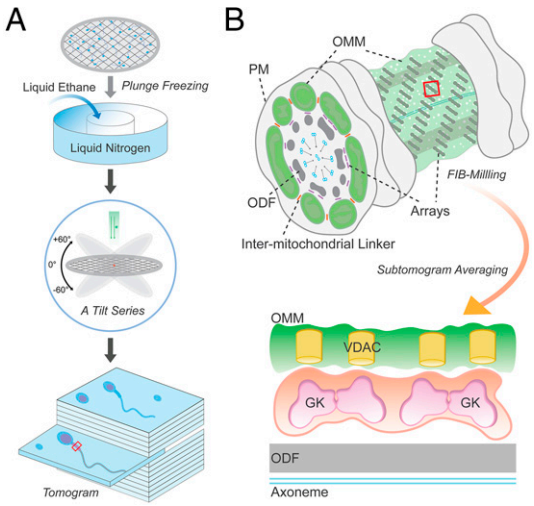

Fig. 1. Supramolecular protein arrays at the mitochondria–cytoskeleton interface in mammalian sperm. (*A*) A schematic cartoon illustrating steps of obtaining a 3D reconstruction image of a plunge-frozen sperm using cryo-ET. A small volume of a suspension of sperm cells is placed onto a carbon grid and then plunge frozen in liquid ethane cooled to temperatures of ~100 K by liquid nitrogen. The grid is then transferred into the column of an electron microscope for collection of a series of images at varying tilts. The series of tilted images is then converted to a 3D volume (tomogram) that provides a representation of the distribution of EM densities of cellular components. (*B*) A part of the midpiece from a mammalian sperm depicting a flagellar cross-section and an exposed mitochondria–cytoskeleton interface studded with the protein arrays. Intermitochondrial linkers are marked in orange. FIB milling can generate thin slices exposing the area of interest for subtomogram averaging. PM, plasma membrane; ODF, outer dense fiber.

presents three distinct surfaces with two interaction sites for each mitochondrion to face (i.e., intermitochondria and mitochondrial–cytoskeleton contacts)

[a]Department of Cellular & Molecular Physiology, Yale School of Medicine, New Haven, CT 06510; and [b]Department of Obstetrics & Gynecology, Yale School of Medicine, New Haven, CT 06510

Author contributions: H.W. and J.-J.C. wrote the paper.

The authors declare no competing interest.

See companion article, "In-cell structures of conserved supramolecular protein arrays at the mitochondria–cytoskeleton interface in mammalian sperm," 10.1073/pnas.2110996118.

[1]To whom correspondence may be addressed. Email: jean-ju.chung@yale.edu.

Published November 24, 2021.

(Fig. 1*B*). Earlier studies using freeze-fracture EM and thin-section EM on guinea pig (10) and golden hamster (11) sperm revealed unique membrane profiles for each surface. These studies described the high-order protein arrays on the cytoskeleton-facing surface of mitochondria for the first time. Later, the advent of mouse genetics toolkits helped in observing abnormal mitochondrial morphology and disorganized mitochondrial sheaths in sperm from various infertile mutant mice, hinting at the molecular landscape and physiological significance. Voltage-dependent anion channel 3 (VDAC3) (12) and sperm-specific isoforms of glycerol kinase (GK) (13, 14) were added to the list of these key molecules in the assembly and/or structure of the mitochondrial sheath. However, the exact molecular identity of these arrays and how they anchor onto the outer mitochondrial membrane (OMM) with a particular orientation have remained unknown.

Leung et al. (8) now reveal the three-dimensional (3D) structures of these arrays at molecular resolution by cryoelectron tomography (cryo-ET), a type of cryo-EM. The unique advantage of cryo-EM over conventional EM and fluorescence light microscopy is that cryo-EM can image in a near-native state. The sample processing does not involve chemical fixatives or stains, preserving cellular context and high-order assembly close to physiological state. In a nutshell, the sample freezes so fast at cryogenic temperature that ice crystals cannot form, thus being trapped in vitreous (glass-like) ice (Fig. 1*A*). Averaging individual particles in such thin, vitreous ice generates high-resolution structures of purified proteins and protein complexes (i.e., single-particle analysis). Yet, even small cells like mammalian sperm are too immense and complex for direct averaging. Thus, a preferable cellular cryo-EM is cryo-ET in which freeze fixation is combined with multiangle EM imaging to provide a high-resolution 3D volume reconstruction of the original object (i.e., tomogram) (Fig. 1*A*). More recently, cryo-focused ion beam (cryo-FIB) milling which cuts out 150- to 200-nm thin slices (called "lamellae") of the sample has enabled higher-resolution tomographic reconstructions. In particular, highly repetitive structures in a tomogram can be further aligned and averaged—subtomogram averaging—to enhance the signal-to-noise ratio, ideally achieving near-atomic resolution. Therefore, cryo-ET and subtomogram averaging provide molecular resolution maps of protein complexes in the cellular context (15).

The strength of the study by Leung et al. (8) lies in their use of this multiscale cryo-ET approach to sperm mitochondria from three mammalian species—pigs, horses, and mice—that rely on mitochondrial respiration for energy production to different extents (15). Thus, differences and similarities observed from this comparative structural study (8) can provide insights into the conservation and divergence of mitochondrial organization in sperm metabolism and motility. For example, their study finds linker complexes between the outer membrane of neighboring mitochondria in all three species. It is not yet clear whether these linkers are specific to mammalian sperm mitochondrial organization or are more general structures analogous to those seen in other somatic cells. Another striking observation, and the main structural focus of this study, is the highly similar average dimensions of individual particles in the highly ordered protein arrays, suggesting conserved supramolecular arrangement. This approach, backed up by proteomics and in-cell cross-linking mass spectrometry of VDACs residing in the OMM, has allowed the authors to present a compelling model for the ladder-like protein arrays. Among the list of candidate VDAC-associated proteins, GK—likely two end-to-end dimers—fit into the boat-shaped EM density that interacts with the pores, consistent with those of VDACs. These arrays orient toward the flagellar cytoskeleton, and thus likely need interaction with the submitochondrial reticulum which is cytoskeletal filaments yet to be characterized (Fig. 1*B*). The ubiquitous expression of VDACs in OMM also raises a possibility that the ordered protein arrays comprising GK serve as universal regulatory and/or structural mechanisms at the mitochondria–cytoskeleton interface across species or cell types.

In summary, the study by Leung et al. uses FIB-milling-enabled cryo-ET to image mammalian sperm. Subsequent subtomogram averaging resolved in-cell structure of the ordered protein arrays in sperm mitochondria–cytoskeleton contacts from three mammalian species.

In contrast, differences observed in the sperm mitochondria among the three species might reflect species-specific sperm metabolism in pursuit of fertilization. Any change in sperm morphology can affect sperm performance, thus leading to directional evolution of the fertilization system. In amniotes that fertilize internally (e.g., birds and mammals), sperm display an extensive mitochondrial sheaths, a likely adaptation to power the large, long flagellum in these lineages. Accordingly, variations in midpiece morphometry have been implicated in affecting sperm motility and competitiveness (17). Leung et al. (8) observe that mitochondrial dimensions are variable across species but consistent within species. Mouse sperm mitochondria is about 1.5 to 2 times wider than those in pig and horse sperm. This difference in mitochondrial dimension presumably corresponds to a longer midpiece in mouse sperm compared to pig and horse sperm, which keeps the total mitochondrial number within a similar range. More intriguing is the ultrastructural differences in the internal organization of mitochondria. Horse sperm mitochondria have a condensed matrix and an expanded intermembrane space. By contrast, mouse sperm display an expanded matrix but a narrower intermembrane space with more-defined, thin cristae. Additionally, only mouse sperm exhibit cristae aligned across two neighboring mitochondria (i.e., transmitochondrial cristae), like those in muscle tissue proposed to electrochemically couple adjacent mitochondria (18). These differences suggest different energy partitioning between glycolysis and oxidative phosphorylation in sperm metabolism. Horse spermatozoa were previously reported to require higher oxidative phosphorylation for maintaining motility than pig and mouse sperm which both are largely dependent on glycolysis (16). However, it was previously shown that mouse sperm lacking the major Ca^{2+} clearance protein (plasma membrane calcium ATPase 4, PMCA4)—thus, experiencing Ca^{2+} overload—contain condensed mitochondria and cannot hyperactivate (19). Moreover, mitochondrial cristae organization was reported to determine respiratory efficiency, as cristae shape and ATPase dimers are linked (20). These results complicate direct association of the structural features to mitochondrial energetics. Considering that recent findings show mouse sperm cells begin to increase oxidative phosphorylation during capacitation (21), it will be an interesting approach to see whether and what changes in mitochondrial structures would occur during sperm capacitation in a given species.

In summary, the study by Leung et al. (8) uses FIB-milling-enabled cryo-ET to image mammalian sperm. Subsequent subtomogram averaging resolved in-cell structure of the ordered protein arrays in sperm mitochondria–cytoskeleton contacts from three mammalian species. The current results support and expand earlier investigations by revealing the conserved structure at molecular resolution. Importantly, this paper raises questions for further studies. First, it provides a compelling supramolecular model of GK–VDAC shuttling potential metabolites en route from mitochondria to the axoneme. Second, it suggests that structural changes in cristae or intermitochondrial junctions reflect changes in metabolic demand, such as during sperm capacitation. Finally, it illustrates how cellular cryo-EM approach can allow for studying other supramolecular structures in sperm.

Acknowledgments

This work was supported by National Institute of Child Health and Development of the NIH Grant HD096745.

1 K. R. Porter, A. Claude, E. F. Fullam, A study of tissue culture cells by electron microscopy: Methods and preliminary observations. *J. Exp. Med.* **81**, 233–246 (1945).
2 G. E. Palade, An electron microscope study of the mitochondrial structure. *J. Histochem. Cytochem.* **1**, 188–211 (1953).
3 D. W. Fawcett, A comparative view of sperm ultrastructure. *Biol. Reprod. Suppl.* **2**, 90–127 (1970).
4 J. J. Chung *et al.*, Structurally distinct Ca^{2+} signaling domains of sperm flagella orchestrate tyrosine phosphorylation and motility. *Cell* **157**, 808–822 (2014).
5 L. Ded, J. Y. Hwang, K. Miki, H. F. Shi, J. J. Chung, 3D in situ imaging of the female reproductive tract reveals molecular signatures of fertilizing spermatozoa in mice. *eLife* **9**, e62043 (2020).
6 E. L. Fishman *et al.*, A novel atypical sperm centriole is functional during human fertilization. *Nat. Commun.* **9**, 2210 (2018).
7 M. Le Guennec *et al.*, A helical inner scaffold provides a structural basis for centriole cohesion. *Sci. Adv.* **6**, eaaz4137 (2020).
8 M. R. Leung *et al.*, In-cell structures of conserved supramolecular protein arrays at the mitochondria–cytoskeleton interface in mammalian sperm. *Proc. Natl. Acad. Sci. U.S.A.* **118**, e2110996118 (2021).
9 A. S. Moore, E. L. F. Holzbaur, Mitochondrial-cytoskeletal interactions: Dynamic associations that facilitate network function and remodeling. *Curr. Opin. Physiol.* **3**, 94–100 (2018).
10 D. S. Friend, J. E. Heuser, Orderly particle arrays on the mitochondrial outer membrane in rapidly-frozen sperm. *Anat. Rec.* **199**, 159–175 (1981).
11 G. E. Olson, V. P. Winfrey, Structural organization of surface domains of sperm mitochondria. *Mol. Reprod. Dev.* **33**, 89–98 (1992).
12 M. J. Sampson *et al.*, Immotile sperm and infertility in mice lacking mitochondrial voltage-dependent anion channel type 3. *J. Biol. Chem.* **276**, 39206–39212 (2001).
13 Y. Chen *et al.*, Glycerol kinase-like proteins cooperate with Pld6 in regulating sperm mitochondrial sheath formation and male fertility. *Cell Discov.* **3**, 17030 (2017).
14 K. Shimada, H. Kato, H. Miyata, M. Ikawa, Glycerol kinase 2 is essential for proper arrangement of crescent-like mitochondria to form the mitochondrial sheath during mouse spermatogenesis. *J. Reprod. Dev.* **65**, 155–162 (2019).
15 M. Beck, W. Baumeister, Cryo-electron tomography: Can it reveal the molecular sociology of cells in atomic detail? *Trends Cell Biol.* **26**, P825-837 (2016).
16 M. P. Davila *et al.*, Mitochondrial ATP is required for the maintenance of membrane integrity in stallion spermatozoa, whereas motility requires both glycolysis and oxidative phosphorylation. *Reproduction* **152**, 683–694 (2016).
17 H. S. Fisher, E. Jacobs-Palmer, J. M. Lassance, H. E. Hoekstra, The genetic basis and fitness consequences of sperm midpiece size in deer mice. *Nat. Commun.* **7**, 13652 (2016).
18 M. Picard *et al.*, Trans-mitochondrial coordination of cristae at regulated membrane junctions. *Nat. Commun.* **6**, 6259 (2015).
19 G. W. Okunade *et al.*, Targeted ablation of plasma membrane Ca2+-ATPase (PMCA) 1 and 4 indicates a major housekeeping function for PMCA1 and a critical role in hyperactivated sperm motility and male fertility for PMCA4. *J. Biol. Chem.* **279**, 33742–33750 (2004).
20 S. Cogliati *et al.*, Mitochondrial cristae shape determines respiratory chain supercomplexes assembly and respiratory efficiency. *Cell* **155**, 160–171 (2013).
21 M. Balbach *et al.*, Metabolic changes in mouse sperm during capacitation. *Biol. Reprod.* **103**, 791–801 (2020).